

UC Davis

UC Davis Previously Published Works

Title

Disrupted brain mitochondrial morphology after in vivo hydrogen sulfide exposure

Permalink

<https://escholarship.org/uc/item/27k0x6kj>

Journal

Scientific Reports, 13(1)

ISSN

2045-2322

Authors

Rumbeiha, Wilson K
Kim, Dong-Suk
Min, Angela
et al.

Publication Date

2023-10-01

DOI

10.1038/s41598-023-44807-y

Copyright Information

This work is made available under the terms of a Creative Commons Attribution License, available at <https://creativecommons.org/licenses/by/4.0/>

Peer reviewed



OPEN

Disrupted brain mitochondrial morphology after in vivo hydrogen sulfide exposure

Wilson K. Rumbeiha¹✉, Dong-Suk Kim¹, Angela Min^{1,3}, Maya Nair^{1,3} & Cecilia Giulivi^{1,2}✉

Changes in mitochondrial dynamics are often associated with dietary patterns, medical treatments, xenobiotics, and diseases. Toxic exposures to hydrogen sulfide (H₂S) harm mitochondria by inhibiting Complex IV and via other mechanisms. However, changes in mitochondrial dynamics, including morphology following acute exposure to H₂S, are not yet fully understood. This study followed mitochondrial morphology changes over time after a single acute LCt₅₀ dose of H₂S by examining electron microscopy thalamic images of surviving mice. Our findings revealed that within the initial 48 h after H₂S exposure, mitochondrial morphology was impaired by H₂S, supported by the disruption and scarcity of the cristae, which are required to enhance the surface area for ATP production. At the 72-h mark point, a spectrum of morphological cellular changes was observed, and the disordered mitochondrial network, accompanied by the probable disruption of mitophagy, was tied to changes in mitochondrial shape. In summary, this study sheds light on how acute exposure to high levels of H₂S triggers alterations in mitochondrial shape and structure as early as 24 h that become more evident at 72 h post-exposure. These findings underscore the impact of H₂S on mitochondrial function and overall cellular health.

The brain orchestrates complex cognitive functions and vital physiological processes. Central to the brain's remarkable abilities are mitochondria, the cellular powerhouses responsible for generating the majority of adenosine triphosphate (ATP), the cell's energy currency. These organelles are crucial in maintaining cellular homeostasis, regulating apoptosis, and serving as a pivotal interface in the brain's response to various environmental stimuli. Hydrogen sulfide (H₂S) is a common environmental toxicant and a crucial gaseous molecule naturally produced in the body¹, including the brain².

The morphology and function of mitochondria in the brain have become subjects of increasing interest in scientific research. Recent investigations have revealed that mitochondrial dynamics and their structural adaptations can influence neuronal health, synaptic plasticity, and overall cognitive performance^{3–6}. Proper mitochondrial function is essential for sustaining neural activities, while its dysfunction may lead to neurodegenerative diseases and cognitive impairments^{7–9}. Mitochondria typically have an elongated shape, delimited by smooth outer and complex inner membranes¹⁰. The tight and structured packing of the infoldings of the inner membrane (cristae) is functionally essential for increasing the surface area for ATP production^{11–13}. The *intermembrane space*¹⁴ is located between the inner and outer membranes, whereas the *matrix* is the space inside the inner membrane. The latter subcompartment contains critical organic and inorganic compounds, biomolecules (mitochondrial DNA), soluble enzymes of the citric acid cycle, and structures (matrix granules, ribosomes)¹⁴. Notably, the size (~0.5 to 3 μm), shape, and number of mitochondria vary considerably between cell types, developmental stage, age, and environmental factors, among others, and even within the chondriome¹⁵. The preservation of this dynamic homeostasis is critical for mitochondria to adapt to changing living conditions. As such, mitochondria in cells move, change shape, and fuse or split¹⁶ in a process called mitochondrial dynamics. This process is essential for maintaining their shape, distribution, and size; alterations of any of these are associated with numerous human diseases¹⁷.

In recent decades, the harmful effects of environmental pollutants on brain health have garnered considerable attention. One such environmental hazard is H₂S. Once known solely for its toxic properties^{18,19}, H₂S has emerged as a remarkable gasotransmitter with versatile physiological functions in recent years^{20–22}. H₂S is now recognized as a key signaling molecule involved in diverse cellular processes, including vasodilation,

¹Department of Molecular Biosciences, School of Veterinary Medicine, University of California Davis, Davis, CA, USA. ²Medical Investigation of Neurodevelopmental Disorders (MIND) Institute UCDH, University of California Davis, Sacramento, CA, USA. ³These authors contributed equally: Angela Min and Maya Nair. ✉email: wkrumbeiha@ucdavis.edu; cgiulivi@ucdavis.edu

inflammation, cognition, and neurotransmission. While the biochemistry and signaling roles of endogenous H₂S continue to be extensively studied, its effects on cellular organelles, especially mitochondria, which are a well-known target for H₂S-induced toxicity, have gained increasing attention. The intricate crosstalk between H₂S and mitochondria has sparked considerable interest among researchers, as mounting evidence suggests that H₂S may modulate mitochondrial morphology and function in a dose–response association, from signaling to toxic, detrimental health effects.

This study explored the fascinating interplay between a single acute H₂S exposure and changes in brain mitochondrial morphology, shedding light on the potential implications for cellular health and disease. Only one other study indicated qualitative changes in mitochondria morphology in the brains of a rat model of alcoholism treated with aminooxyacetic acid (an inhibitor of cystathionine-beta-synthase) that increases endogenous H₂S levels²³, but not acute exposures. Here, we sought to elucidate the potential mechanisms through which H₂S may influence mitochondrial dynamics in the brain. To this end, we analyzed 123 images obtained from the brains of mice exposed to 1000 ppm H₂S for 30 min, and cohorts of surviving mice were sacrificed at 12, 24, 48, and 72 h post-exposure to generate a detailed picture of changes over time in mitochondrial morphology in murine thalamus. This dose was chosen to mimic acute H₂S exposure following industrial accidents or nefarious acts^{24,25}. The thalamus was explored as it is one of the most sensitive brain regions upon H₂S acute exposure¹⁹. Understanding the complex interplay between mitochondria and H₂S is essential for advancing our knowledge of neurobiology and environmental health, including neurodegeneration, and identifying potential therapeutic targets and strategies to mitigate the adverse effects of environmental pollutants on brain function. By shedding light on this critical intersection between cellular biology and environmental factors, this research may pave the way for novel interventions to safeguard brain health in an increasingly polluted world.

Results

Young adult C57BL/6 J male mice, aged 7–8 weeks, were randomly allocated to the (exposed) H₂S group ($n = 12$) and the room air group (control; $n = 4$), following a protocol previously documented^{26,27}. The exposed mice were subjected to a single inhalation dose of H₂S at 1000 ppm for 30 min, while the control group was exposed to room air through whole-body exposure. This H₂S concentration was chosen because it replicates an acute H₂S exposure scenario resembling accidental or intentional releases of this toxic gas^{24,28–30}. This exposure results in a 50% mortality rate, known as LC₅₀. Euthanasia of the surviving mice occurred at the following time points: 12, 24, 48, and 72 h post-exposure and their brains were promptly extracted and processed for electron microscopy to assess the impact of H₂S on mitochondrial morphology (exposure paradigm shown in Fig. 1A). The focus on mitochondria was based not only on the role of this organelle in the CNS³¹, and the more potent inhibition of cytochrome *c* oxidase by H₂S than cyanide³², but also because 50 mg/kg NaHS-treated mice showed a threefold and twofold increase in sulfides in myelin and mitochondria, respectively, compared to control animals³³.

Representative images from transmission electron microscopy (TEM) of thalami from air-breathing animals show neuronal elements with well-preserved subcellular organelles (Fig. 1B, C). The rough endoplasmic reticulum (RER), and mitochondrial and cellular membranes are intact. The lysosomes and Golgi complexes are well preserved. Myelin sheaths show normal compaction with occasional loosening of myelin wraps. Nuclei show normal euchromatin. There is a scatter of electron-dense myeloid bodies in the neuropils.

In general, the inspection of the TEM images from H₂S-exposed mice revealed a phenotype consistent with that of tissues affected by hypoxia, ischemia, and chemical hypoxia, akin to cyanide poisoning. At 12 h, mitochondria vacuolization, swelling, and cristae disruption are evident (Fig. 1D). Swollen mitochondria were identified by their expanded matrix space, fewer cristae, and less dense matrix staining. While these changes were observed as early as 12 h, those at 72 h were the most evident (Fig. 1D, F).

In some cases, the cristae were pushed to the side, and an amorphous material was present (likely unfolded, damaged proteins; Fig. 1F). Golgi complexes were swollen and disorganized (Fig. 1E). Lysosome and RER were enlarged following 72 h post-H₂S exposure (Fig. 1E). At 72 h, neural soma cytoplasm showed rarefaction with aggregation of cytoplasmic contents and dilated endoplasmic reticulum (E.R; shown with asterisks; Fig. 1E). The neuropil contained axons, and neuronal nuclei are hypodense.

At 48 h, mitochondria fission was increased, possibly in an attempt to clear damaged mitochondria by mitophagy (Fig. 2A). However, this process seemed halted later with the presence of elongated, longer mitochondria at 72 h (Fig. 2B). Although these mitochondria have a larger size and elongation, they do not seem to be functional, as their cristae are sparse or loosely packed (Fig. 2B). Vacuolization of mitochondria was more evident at 72 h and observed as a loss of structured cristae, invaginations of the inner membrane, and matrix components accumulated to the side of the mitochondrial body (Fig. 2B).

At time points 48 h and 72 h, the degree of mitochondrial damage was more evident than at 12–24 h, accompanied by dilation of RER cisternae (loss and disruption of Golgi apparatus), loss of organized ribosomes on RER, large aggregates of smooth endoplasmic reticulum, presence of single-membrane vacuoles, and autophagosomes with lipid material (Fig. 3A–C).

At 24 h after H₂S exposure, a few double-membrane autophagosomes with engulfed organelles were observed (Fig. 3A, blue circle). But at 72 h, C-shaped double membrane structures (arrow) or double-membrane vacuoles (V) were observed. Note at this time point, cytoplasm vacuolization was apparent (Fig. 3B), and lipid droplets phagocytized by lysosomes were visible and stained dark (arrowheads; Fig. 3C). Notably, lipid droplets are a well-documented source for the maintenance of mitochondrial membrane integrity and fatty acids for mitochondrial fatty acid β oxidation and have more recently been shown to play a protective role in the sequestration of toxic lipids that arise during autophagic degradation of membranous organelles³⁴.

We performed a qualitative analysis of TEM images on the myelin structure because relatively high sulfide content in myelin- and mitochondrial-enriched fractions was previously reported in mice dosed with 50 mg/kg

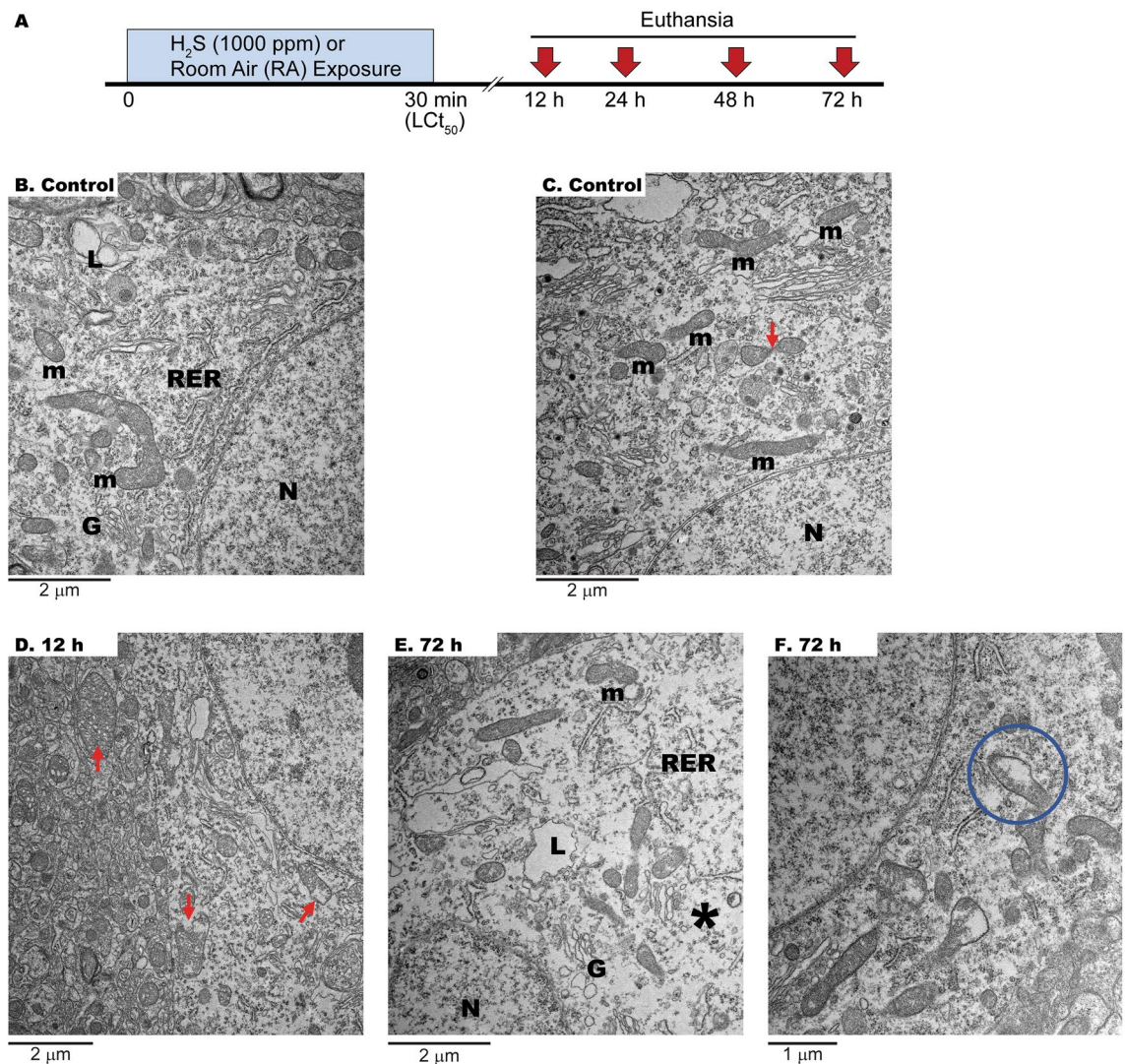


Figure 1. Experimental protocol and neuronal changes after acute H₂S exposure. **(A)** A diagram summarizing the experimental procedure. Mice were exposed once to H₂S at 1000 ppm for 30 min. Cohorts of surviving mice were euthanized at 12, 24, 48 and 72 h post-exposure. **(B,C)** Normal appearance of cytoplasm, organelles, and nucleus (N) in control brain samples from a mouse exposed to room air (normal mitochondria marked with m). **(D)** As early as 12 h after H₂S exposure, mitochondria displayed swelling, dilation, and vacuolization (arrows). **(E,F)** At 72 h, significant cristae disruption was observed (circle marks magnification) with amorphous proteinaceous material, possibly resulting from unfolded, damaged proteins. The cytoplasm is rarefied (asterisk). RER rough endoplasmic reticulum, m mitochondria, G Golgi apparatus, L lysosomes.

NaHS³³. Quantitative analysis of myelin thickness (for example ³⁵) was not performed as it varies with neuron types within the brain region requiring specific staining for identifying the neuron type and biomarkers of myelin proteins. Under control conditions, myelin was well-developed, with a compact structure with axons enclosed in myelin visible (indicated by the arrows), and the layers exhibited a highly organized appearance (Fig. 4A). In the H₂S-exposed group, many small vacuoles were observed in the myelin at 24 h (Fig. 4B), 48 h (not shown), and 72 h (asterisks; Fig. 4C). Myelin exhibited a loose structure and an increased inter-layer gap with visible stratification, which indicated a disrupted packing (thin arrows; Fig. 4C).

Characterization of brain mitochondria after H₂S exposure

Using ImageJ software, quantitative measurements of morphometric parameters (surface area, perimeter, roundness, density, aspect ratio, and form factor) were performed on mitochondria from the TEM images (Fig. 5). Each panel contains the 95% confidence interval of control values (grey boxes). Values outside the 95%CI were considered abnormal. The area of mitochondria in the brains of H₂S-exposed animals at 12 and 24 h post-exposure was higher and lower (respectively) than controls (air-breathing animals; Fig. 5A). At 72 h, the area of mitochondria from H₂S-exposed mice was generally larger than that from control mice (Fig. 5A). A similar trend was observed for the perimeter (Fig. 5B). The density of mitochondria was higher at 12 h than control animals, followed by a significant dip at 24 h, and similar to the area outcome, reverting to almost control values by 72 h (Fig. 5C).

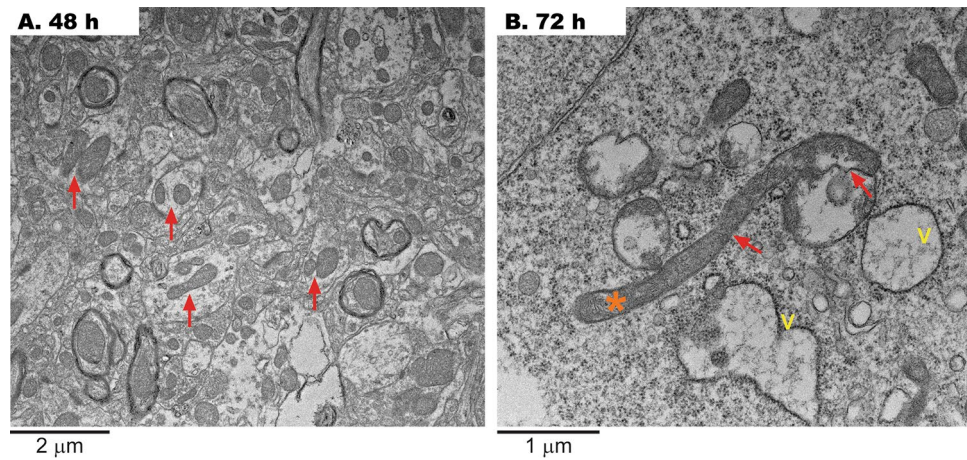


Figure 2. Late disruption of brain mitochondria fission after acute H₂S exposure. **(A)** At 48 h, active fission was observed (arrows) to enhance mitophagy's clearance of damaged mitochondria. **(B)** At 72 h, the fission process seems halted, as judged by the appearance of long, damaged mitochondria (asterisk).

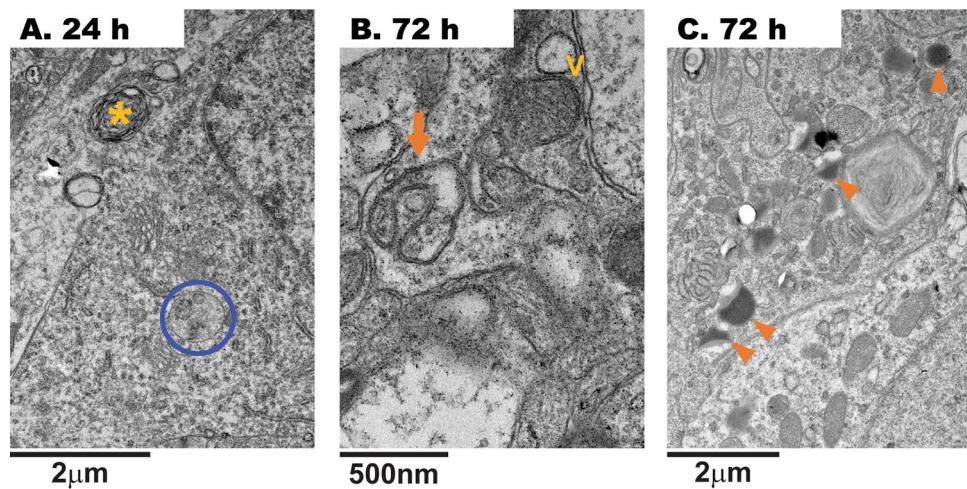


Figure 3. Generalized brain lesions after acute H₂S exposure. **(A)** At 24-h after H₂S exposure, a few double-membrane autophagosomes with engulfed organelles were observed (blue circle). **(B)** At 72-h, C-shaped double membrane structures (arrow) or double-membrane vacuoles (V) were observed. **(C)** At 72-h after H₂S exposure, lipid droplets phagocytized by lysosomes were visible and stained dark (arrowheads). Both apoptotic and necrotic morphological features were seen (cell shrinkage, large chromatin clumps, damaged organelles, and deteriorated membranes).

As the change from elongated to smaller, round mitochondria indicates fragmentation and cellular stress^{36,37}, we assessed mitochondrial roundness as a surrogate for evaluating the extent of mitochondrial fragmentation. These data span from 0 to 1, with 1 being a perfect circle. Mitochondria from H₂S-exposed animals at 12 h showed increased roundness compared to controls (Fig. 5D), whereas a steady increase in roundness was also observed at later time points. These results indicated a significantly increased early mitochondrial fragmentation at 12 h followed by a steady decrease in fragmentation at 48 h and later.

Finally, mitochondrial branching and network were assessed in the images. In response to stress, mitochondria can adapt in a short timeframe to increase ATP production (e.g., calcium-dependent activation of specific dehydrogenases within the citric acid cycle³⁸). In contrast, long-term adaptation may include changes in the chondriome network, content, ultrastructure, and enzymatic levels^{39,40}. As a decrease in mitochondrial network complexity can result from fragmented, rounder mitochondria and increased mitochondrial fission, we calculated the aspect ratio (Fig. 5E) and the form factor (Fig. 5F) to describe the mitochondrial network complexity^{41,42}. Mitochondrial aspect ratio estimates length (i.e., the ratio between major and minor axes of an ellipse equivalent to the mitochondrion). The aspect ratio has a minimal value of 1, corresponding to a circular mitochondrion. The aspect ratio was significantly lower at 12 h (closer to a circle). In comparison to control, at 48 h and later, a trend towards increased roundness was noted (Fig. 5E). These results indicated increased round, circular mitochondria (and less elongated) in response to H₂S exposure.

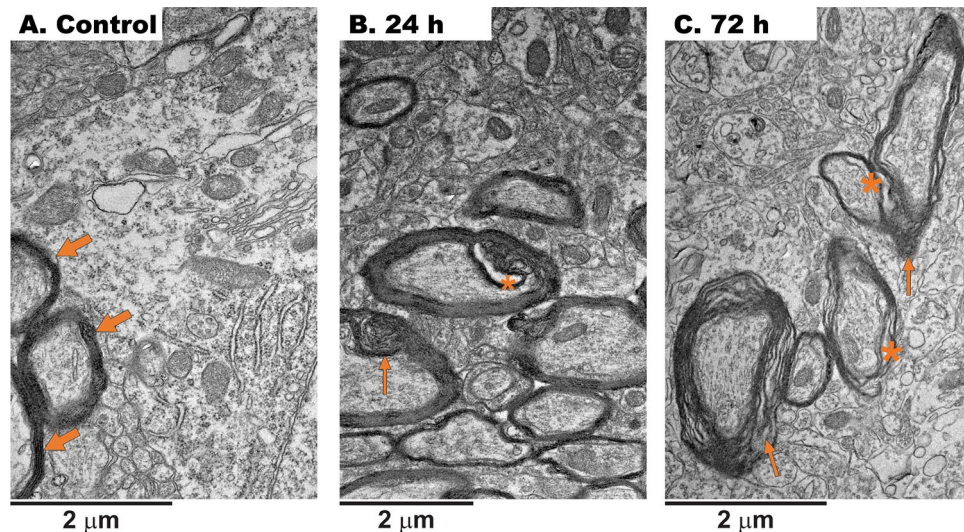


Figure 4. Myelin packing is affected by acute H₂S exposure. (A) Under control conditions, myelin was well-developed, with a compact structure with axons enclosed in myelin visible (indicated by the arrows), and the layers exhibited a highly organized appearance. (B,C) In the H₂S-exposed group, many small vacuoles (not quantified) were observed in the myelin at 24 h, 48 h, and 72 h (asterisks). In (C), myelin exhibited a loose structure and an increased inter-layer gap with visible stratification, which indicated a disrupted development (thin arrows).

The form factor [form factor = $1/4 \times (\text{area}/\text{perimeter}^2)$] is a number that combines measures of length and degree of branching⁴². Mitochondria with large aspect ratios are larger organelles, elongated, whereas those with high form factor scores contain more complex branching⁴². As observed above, exposure to H₂S resulted in a fall of the aspect ratio at 12 h, followed by a steady decline from 24 h and on (Fig. 5E). The form factor scores declined at all time points, with some recovery observed at 72 h, suggesting a disrupted chondriome network (Fig. 5F). These results indicated that exposure to H₂S resulted in rounder mitochondria with altered cristae, likely associated with a disruption in the network.

Excessive mitochondrial fragmentation or ineffective clearance of damaged mitochondria after fission may generate smaller mitochondria. In addition, increases in dumbbell-shaped mitochondria can be explained by incomplete mitochondrial fission (halted or slowed in the final stages of this process) or an overall increase in the total number of mitochondria undergoing fission. Although the number of dumbbell-shaped mitochondria found in each image was insufficient for robust statistical analysis, the distribution of mitochondrial size and mitochondrial density aided the understanding of these options. To this end, we calculated the area distribution (as a surrogate for size; Fig. 6A) and density of mitochondria (Fig. 6B) of control and exposed animals. The values were binned into three categories (below and above the “control range”), considering most mitochondria in control animals as the “control range” (Supplementary Information). The population of smaller mitochondria increased at 24 h, whereas that of larger mitochondria was observed at 12 h and 48 h (Fig. 6A). The distribution of mitochondrial density (integrated density calculated as area \times mean gray value of pixels for each mitochondrion) showed increases in the population with more density (likely clumped material) at 12 h (and 48 h and 72 h). A significant increase in the population of less dense mitochondria is observed at 24 h, likely due to vacuolization (Fig. 6B). Taken together, these results indicated that at 12 h, most mitochondria were larger and denser, whereas at 24 h, they were mostly smaller and less dense; at 48 h, they were larger than at 24 h with less density; at 72 h, they were of sizes comparable to controls but with more representation of denser mitochondria. These results suggested that the fission process of the damaged mitochondria at 12 h was not halted, resulting in smaller and “lighter” mitochondria at 24 h, increasing their sizes by 48 h, and at 72 h, resembling the distribution in size as those of controls but denser (similar to that at 12 h).

Hydrogen sulfide exposure affects morphology and mitochondrial activity

Numerous works^{18,27,43–58}, including publications from Dr. Rumbeih’s team²⁶ have shown decreased cytochrome *c* oxidase activity following acute H₂S exposure of animals. Inhibition of cytochrome *c* oxidase activity reduces ATP production as it is the terminal oxidase of the electron transport chain. Complex IV activity was evaluated in situ in isolated and purified brain mitochondria from mice by using the artificial substrates ascorbate/TMPD in the presence of the Complex III inhibitor antimycin with various concentrations of NaHS as a hydrogen sulfide donor. The range of doses tested was up to 100 μ M which includes the equivalent of brain sulfide after acute exposure to 1,000 ppm H₂S gas, which is approximately equivalent to 15 mg NaHS/kg i.p. (270 μ M NaHS in the bloodstream assuming homogenous distribution; recalculated from³³) and taking into account that at the physiological pH of 7.4, approximately one-third of the sulfide, whether derived from gaseous H₂S or one of its alkali salts, will exist in the form of H₂S (Fig. 6C). The data were presented as a Dixon plot (NaHS

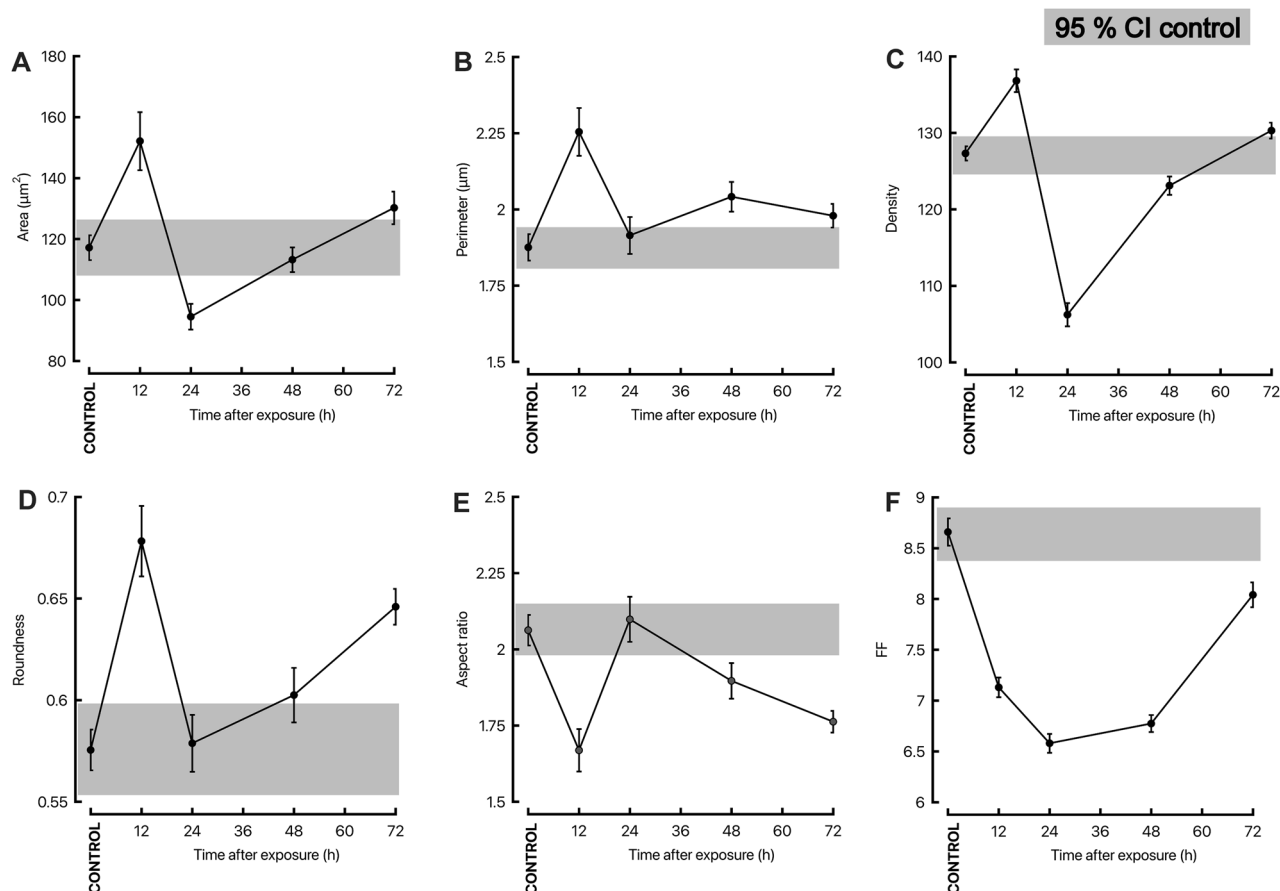


Figure 5. Acute hydrogen sulfide exposure alters mitochondria morphology. Parameters of mitochondrial morphology obtained with ImageJ software were the following: area (A), perimeter (B), density (C), roundness (D), aspect ratio (E), and form factor (F). Average values/conditions with S.D. are presented as a function of time for each of the five outcomes. The 95% confidence intervals built with control values from air-breathing animals are shown as grey rectangles, where the top border is the upper 95% CI limit, and the lower border is the lower 95% CI limit.

concentration vs. reciprocal of the Complex IV activity) because it evaluates whether the inhibitor concentration follows a linear correlation with the reciprocal of the velocity of the activity and the calculation of the K_i . The calculated K_i ($2.5 \mu\text{M}$) was similar to that obtained at pH 8.05 ($2.6 \mu\text{M}^{59}$), consistent with the more basic pH of the mitochondrial matrix (pH $\sim 8.0^{60,61}$) and with the increase in inhibition efficiency with decreasing pH⁵⁹. Thus, an endogenous donor of H_2S at concentrations equivalent to those of an acute exposure inhibited Complex IV activity by 83%, indicating that lower ATP production by mitochondria likely accompanied the changes in morphology. We also recalculated brain Complex IV activity evaluated ex vivo from an identical in vivo, whole animal exposure paradigm²⁶ (Fig. 6C, red round marker). The inhibition of the activity seemed underestimated because it corresponded to a concentration of NaHS of about $40 \mu\text{M}$ vs. the expected one of $\sim 100 \mu\text{M}$, suggesting that the degree of inhibition by H_2S of Complex IV in vivo could be substantially higher, especially when samples are extracted under ambient air from animals exposed to H_2S gas and later stored at -80°C for relatively long times. However, we cannot exclude that the inhibition reported by such studies may reflect other damaging effects on this Complex that do not include the competitive inhibition of this gas on Complex IV activity.

Mitochondrial morphology scores after hydrogen sulfide exposure

To study the classification of mitochondria based on five criteria relative to the control air-breathing mice, we randomly selected 50% of the images/group as representative examples for further detailed structural analyses (Fig. 7). We systematically checked on the following criteria: (1) mitochondrial matrix appearance; (2) mitochondrion shape (round vs. oblong); (3) cristae morphology; (4) intactness of mitochondrial outer membrane; and (5) presence of separation between mitochondrial inner and outer membranes (or lamination). The presence of a negative (detrimental) outcome was considered as zero, whereas a positive (beneficial) one was evaluated as a 1. The sum of these individual scores allowed for obtaining an overall mitochondrial morphology score (from 1, the worst, to 5, the best). These scores were obtained for all mitochondria within each image and averaged per image. Examples of the different aspects of this scoring system are shown in Fig. 7, top panel.

Figure 7 bottom panels summarize the resulting mitochondrial morphology scores obtained at each time point. At 72 h, most mitochondria showed a 34% decrease in the overall mitochondria morphology scores

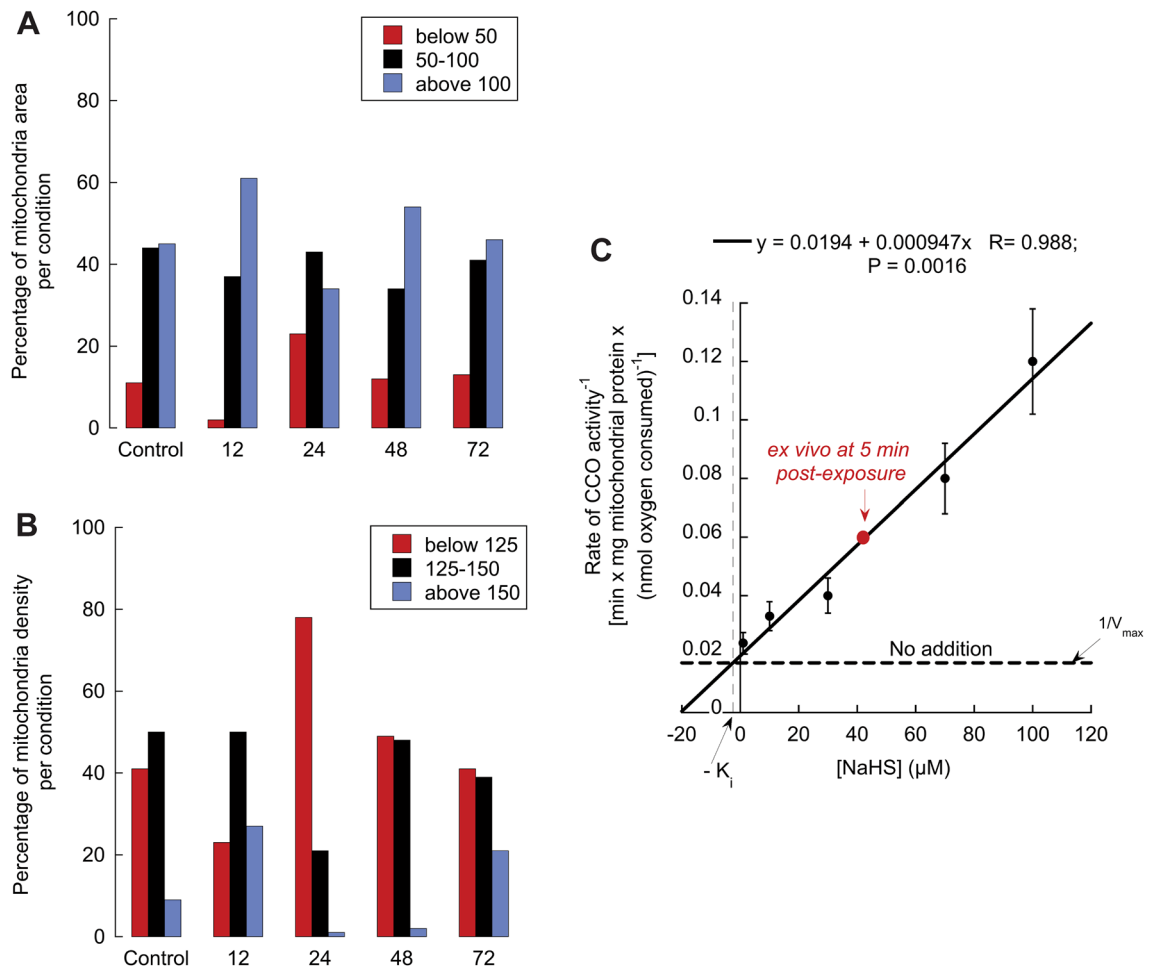


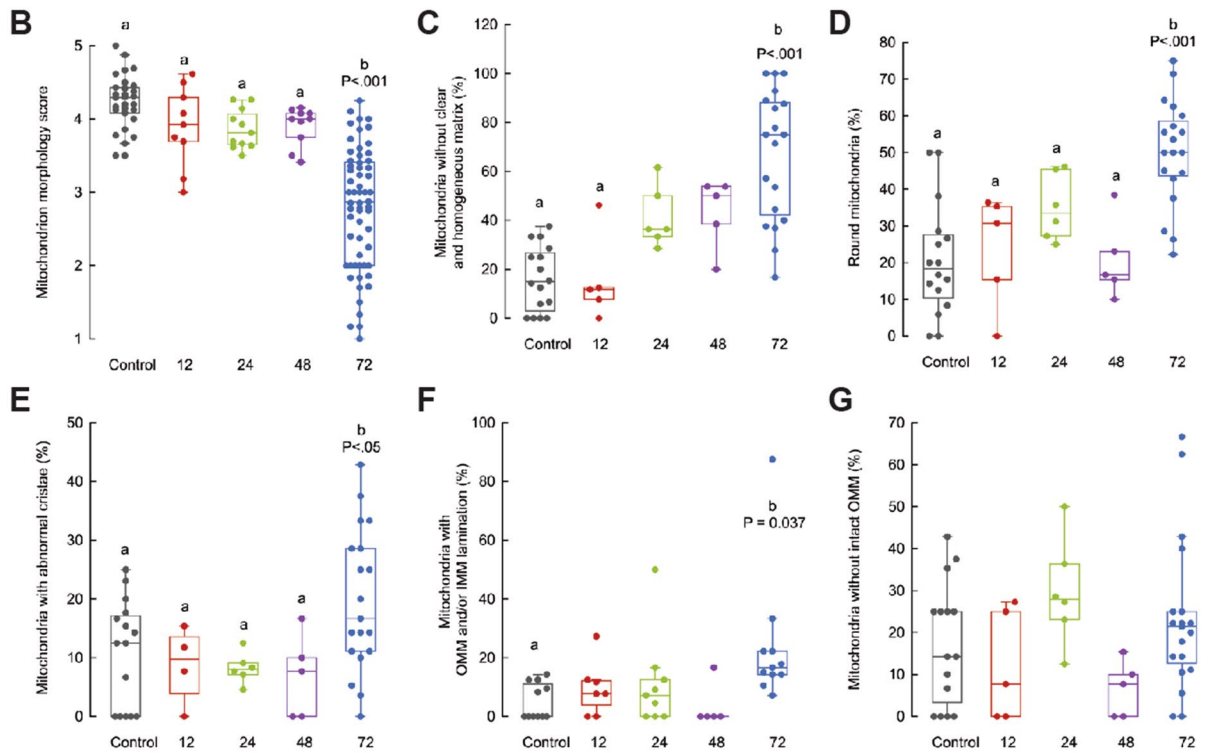
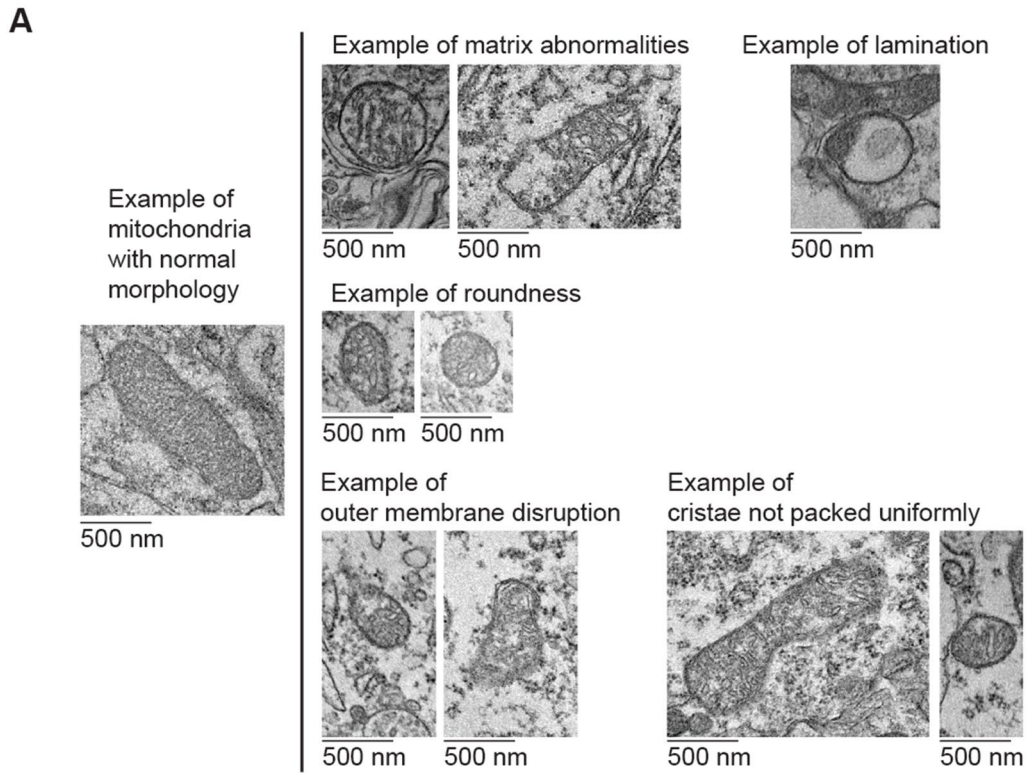
Figure 6. Effect of acute H₂S exposure on the distribution of mitochondrial density and size and Complex IV activity. Values of density and area were obtained for each image and condition using ImageJ. The values were analyzed using JMP software (Supplementary Information). To visualize the effect of H₂S on size (A) and density (B) distributions, range values with the most population from air-breathing animals (black) were taken as “controls”. Values below (red) or above (blue) this range were considered as smaller (size) (or less dense if density), or larger (size) (or denser if density). ImageJ assigns each pixel a value between 0 and 255 depending on the value/color. The integrated density is the sum of all pixel values inside a mitochondrion. It should also equal the (area in pixels)² * mean pixel value (mean grey value). (C) Complex IV activity from rodent brains was evaluated by polarography as indicated in the “Methods”. As a H₂S donor, NaHS was added at the indicated concentrations. Each experiment was done in triplicates, and the data are mean ± SD. The values were presented by using a Dixon plot and fitted to a linear regression (linear regression equation, R value, and Pearson’s P value shown in panel), in which the horizontal dashed line represents 1/V_{max} of Complex IV activity without any NaHS addition. The point at which the fitted line crosses the dashed one, and extrapolated to the X-axis, represents the K_i. The red point represents the ex vivo activity of Complex IV evaluated in brains of mice exposed to the same H₂S paradigm as utilized in this study. Recalculated from ²⁶.

compared to controls (worse; mean ± SEM: 2.8 ± 0.1) than those at all previous time points (for control, 12 h, 24 h, and 48 h, respectively: 4.23 ± 0.07; 3.9 ± 0.2; 3.87 ± 0.08; 3.91 ± 0.08; Fig. 7A).

As the overall score was based on the sum of the scores of the 5 criteria indicated above, we explored whether any particular feature weighted the most towards the lower scores observed at 72 h. This analysis (based on the percentage of mitochondria with a specific feature/image) was relevant as it can provide information on the time course of H₂S’s effect on mitochondrial morphology.

Criterion 1, mitochondrial matrix appearance

This criterion allowed us to assess abnormal accumulations of calcium deposits, clumps, electron-lucent vacuoles, enlarged electron-dense matrix granules, and lipid material in the mitochondrial matrix, indicating impaired quality control mechanisms. Healthy mitochondria rely on efficient mechanisms for removing damaged components through processes like mitophagy, and dysfunctional mitochondria with excessive calcium may evade proper degradation or indicate cellular stress. At 72 h, most (~80%) mitochondria presented enlarged matrix granules, filamentous intramitochondrial crystalline inclusions, and clumped, dense materials compared to



controls or those at 12 h after the exposure (<20%; Fig. 7B), suggesting a decreased space for normal activities of the citric acid cycle and anaplerotic reactions.

Criterion 2, mitochondrial shape

Assessing mitochondria shape (oblong vs. round) allowed for identifying issues with mitochondria dynamics (balance between fission–fusion processes). Imbalances in these processes may lead to mitochondrial dysfunction and have been linked to various diseases, including neurodegenerative disorders. In addition, and as indicated

◀ **Figure 7.** Quantitative comparison of a range of mitochondrial morphometric outcomes obtained after acute H₂S exposure. Top panel. Example of mitochondrial images with disrupted morphology after acute H₂S exposure. Representative images were selected to show the breadth of disrupted mitochondrial morphology assessed in this study. Full details are provided in the main text. Bottom panel. Each data point represents the individual value of a mitochondrion within each condition. Box and whisker plots were used to visualize the spread of data points under each condition. Each box (interquartile distance) encloses 50% of the data, with the median value of the variable displayed as a line. The top and bottom of the box mark the limits of the $\pm 25\%$ of the variable population (i.e., upper and lower quartiles). The lines extending from the top and bottom of the box (whiskers) mark the minimum and maximum values within the dataset that fall within an acceptable range. Any value outside this range, called an outlier, is displayed as an individual point. Mitochondrion morphology score (A) spanning from 1 (worst) to 5 (best). (B–F) The percentage of mitochondria with a particular feature under each condition [abnormal mitochondrial matrix (B), increased roundness (C), abnormal cristae (D), increased lamination (E), and abnormal outer mitochondrial membrane (F)]. ANOVA tests were run for each parameter, followed by Tukey's post-hoc. Equal letters mean no statistical differences.

above, changes in mitochondrial morphology, such as elongation (oblong mitochondria) or fragmentation (round mitochondria), could suggest cellular stress and damage. At 72 h, about half of the mitochondria had a round shape compared to those at previous time points (from 18 to 32%; Fig. 7C). Relevant to the brain, the morphology of mitochondria in neurons is closely linked to synaptic function and plasticity. Healthy neurons often have elongated mitochondria that can efficiently move to the synapses to supply energy and calcium buffering. The increase in round mitochondria in neurons after H₂S exposure may indicate impaired axonal transport or dysfunction. Furthermore, mitochondrial shape and size changes are tightly linked to the process of mitophagy, where damaged or dysfunctional mitochondria are selectively removed. The increase in round mitochondria at 72 h post-exposure may reflect deficiencies in the rates of mitochondrial turnover and mitophagy, essential for maintaining cellular homeostasis.

Criterion 3, cristae morphology

The relevance of assessing cristae morphology relies on evaluating the extensive surface area that provides for the electron transport chain (ETC) and oxidative phosphorylation. These processes are central to synthesizing energy-rich ATP molecules. As such, cristae's organization and morphology directly impact these energy-producing processes' efficiency. Packing cristae and the proximity of components within the ETC facilitate efficient electron transfer and minimize energy loss during mitochondrial respiration. Any cristae morphology and packing alterations can affect the ETC's function, leading to reduced ATP production and increased reactive oxygen species (ROS) generation. Cristae structure also influences the mitochondrial membrane potential, essential for maintaining proper mitochondrial function and regulating cell death pathways.

As observed before, at 72 h post-exposure, a significant number of mitochondria showed disorganized, disrupted cristae, with some showing complete loss of regularly arranged cristae throughout the entirety of the mitochondrial matrix (Fig. 7D). The increased cristae structure disruption after H₂S exposure may point to disruptions in the membrane potential, potentially leading to apoptosis or cellular dysfunction. In addition, as the shape and arrangement of cristae are closely related to mitochondrial dynamics, including fission and fusion events, altered cristae morphology may impact this process, affecting mitochondrial distribution, turnover, and response to cellular stress.

Criterion 4, separation of outer and inner membranes (lamination)

Under this criterion, we recorded mitochondria where the outer and inner membranes were abnormally separated. Many mitochondria at 72 h post-exposure showed displaced cristae with a clear lack of association between inner and outer membranes and an absence of concentric distribution (Fig. 7E). Usually, this feature involves the presence of vacuolization. Similar changes had been observed in other experimental models, such as hypoxia-ischemia^{62,63}. This is consistent with an initial inhibition of oxidative phosphorylation (OXPHOS), followed by abnormal protein synthesis (enlargement of the endoplasmic reticulum).

Criterion 5, intactness of mitochondrial outer membrane

An intact outer membrane is crucial for maintaining the structural integrity of mitochondria as this biological barrier separates the mitochondria from the cytosol, creating a specialized environment for mitochondrial functions and allowing for controlled and compartmentalized biochemical processes within the organelle. In addition, the outer membrane contains various transporters and channels that facilitate the transport of metabolites, ions, and other molecules between the cytosol and mitochondria. The outer membrane also houses the protein import machinery, facilitating nuclear-encoded proteins' transport into the mitochondrial matrix. It also involves signaling and communication between mitochondria and other cellular compartments. For instance, interactions with the endoplasmic reticulum are critical for calcium homeostasis and lipid metabolism. When the outer membrane becomes compromised, it can lead to mitochondrial fragmentation, disrupting mitochondrial dynamics and function and initiating mitophagy. No significant differences were observed in the intactness of the mitochondrial outer membrane across time points after H₂S exposure (Fig. 7F).

Discussion

This study focused on determining the impact of a single acute H₂S exposure on mitochondrial morphology from rodent thalami. The analyses evaluated transmission electron microscope images from mice euthanized at 12, 24, 48, and 72 h after a single acute exposure of 1000 ppm H₂S. This dose was chosen to mimic acute H₂S exposure following industrial accidents or nefarious acts^{24,25,28–30}. Our analysis indicated a rapid metabolic crisis in thalami, evidenced by dramatic changes in mitochondrial morphology ensuing from a single acute exposure to H₂S. The shift in mitochondrial distribution to smaller sizes and the loss of mitochondrial complexity, including cristae, provide solid evidence for injured mitochondria with reduced ATP production. The data on Complex IV activity performed with a H₂S donor at concentrations equivalent to the *in vivo* acute exposure confirmed that hydrogen sulfide exposure (at least at short times after the exposure) is accompanied by morphological changes.

From the morphological assessment, we inferred that the energy-producing capacity of mitochondria, particularly concerning their normal-sized counterparts, is compromised, evidenced by the disorganization and insufficient presence of the inner mitochondrial membrane, where the well-established infoldings known as cristae are found. These cristae play a vital role by increasing the surface area available for ATP production, a key process in cellular energy generation. Upon close examination, it becomes evident that the network within these mitochondria is in disarray, further supporting our conclusion of reduced energy-producing capabilities. The disruption in the organization of the mitochondria likely extends to their ability to undergo mitophagy—the process of recycling and clearing damaged mitochondria from the cell. This disruption in mitophagy can be attributed to changes in the shape of the mitochondria, indicating potential challenges in their clearance and turnover.

While the smaller, rounder mitochondria at early time points may seem targeted for mitophagy, the actual decline in aspect ratio, vacuolization, disrupted matrix, and abnormal cristae at 72 h after H₂S exposure, point to a lingering, halted mitophagy possibly arising from a defective fission–fusion balance. It is known that stress derived from starvation induces an increase in fusion activity resulting in elongated mitochondria to increase the efficiency of the adenosine 5′-triphosphate (ATP) synthesis and protect mitochondria from autophagosomal degradation, thereby enhancing cellular survival during nutrient deprivation⁶⁴. However, if H₂S were to induce elongation or enhance the fusion of mitochondria to escape autophagosomal degradation and enhance ATP production, they should show an increased, intact, and packed cristae structure⁶⁵; however, these elongated mitochondria show cristae sparsely or unevenly arranged (Figs. 2B, 5, 6A, B) suggesting that their presence is not the result of an attempt to compensate the energy deficit or mitophagy. The larger size may be ascribed to significant mitochondrial swelling which occurs only after the loss of mitochondrial membrane potential ($\Delta\Psi_m$) and long after the release of cytochrome *c*⁶⁶. Taking into consideration the disruption of the matrix and cristae structures and the lack of statistically significant outer membrane damage, it is tempting to propose that the early origins of disrupted mitochondria morphology upon acute H₂S exposure reside at the matrix and inner membrane consistent with the early inhibition of Complex IV by H₂S⁵⁰ and increased oxidative stress-mediated damage^{67,68}.

Results also show that acute H₂S exposure significantly injured neuronal myelin sheaths, and endoplasmic reticulum. Myelin sheaths were split and edematous, and axons were rarified and dilated. These neuronal changes corresponded to time course changes noted in mitochondrial morphology. Mitochondrial swelling was notable at the earliest observation time (12 h), and injury was even more evident at 72 h. These results suggest that a single acute exposure to H₂S triggers a cascade of events that lead to mitochondrial injury. As mitochondrial damage worsened (72 h), so did injury of other neuronal cellular components, including the endoplasmic reticulum, Golgi complex, lysosomes, and myelinated sheaths (Figs. 1D, E, 4B, C).

Limitations of this study included (i) the use of male mice only, which precluded the evaluation of the sex effect on H₂S intoxication as others have reported^{45,69}, (ii) the analysis performed on surviving mice which may bias the results assuming unperceived advantages to acute exposure, and (iii) the putative extrapolation to humans considering species differences⁷⁰ and similarities^{71,72} including the use of 7–8 weeks old mice (considered as young adults) whose maturational rate does not linearly correlate with humans. Finally, the substrain C57BL/6J has negligible mitochondrial nicotinamide transhydrogenase activity due to a deletion comprising the *Nnt* gene⁷³, and as such, an increased background of mitochondrial oxidative stress^{73,74}, which may have resulted in the presentation of a more severe phenotype.

In conclusion, our findings show that acute exposure to 1000 ppm of H₂S for 30 min (LC₅₀) directly impacts the structural integrity and functional efficiency of mitochondria from thalami. This is primarily manifested through the disorganization and scarcity of the inner mitochondrial membrane. Furthermore, the altered network organization and compromised mitophagy accentuate the challenges these mitochondria face in maintaining optimal energy production and cellular health. This comprehensive exploration of the interactions between H₂S exposure and mitochondrial morphology aims to contribute to the growing knowledge surrounding the intricate crosstalk between friend H₂S gasotransmitter and foe H₂S xenobiotic on cellular organelles. The findings from this study may pave the way for novel therapeutic strategies harnessing the potential of H₂S to modulate mitochondrial function (e.g., activate mitophagy), thus offering new avenues for improving overall cellular health.

Materials and methods

Animals

All animal studies were approved by the Institutional Animal Care and Use Committee (IACUC-18-136, Feb. 2019) of Iowa State University (ISU). This study is fully aligned with the ARRIVE 2.0 guidelines⁷⁵, ensuring transparent and comprehensive reporting of the research methods utilized in this study and its outcomes. Adhering to these guidelines enhances research quality and reproducibility, underscoring our commitment to upholding rigorous standards and promoting transparency in our findings. We confirm that all experiments were performed in accordance with relevant guidelines and regulations. Animals were treated humanely and handled with care. The 7–8-week-old male C57BL/6J mice were purchased from the Jackson Laboratories (Bar Harbor, ME). Mice

were housed in five per cage in the laboratory animal resources (LAR) at the College of Veterinary Medicine, ISU, with a 12:12 h light and dark cycle. Room temperature and relative humidity were maintained at 22 °C and 35–50%, respectively. Protein Rodent maintenance diet (Teklad HSD Inc., WI) and drinking water were provided ad libitum. Mice were acclimated for at least 72 h before the start of the experiments.

Exposure paradigm

C57BL/6J male mice 7–8 weeks old (considered young adults) were randomly assigned to each group ($n = 12$ for the H₂S-breathing group and $n = 4$ for the control or ambient air-breathing group), following a protocol published before^{26,27}. The experimental protocol is summarized in Fig. 1A. Mice were exposed to a single dose of H₂S at 1000 ppm (exposed) or room air (control) by inhalation (whole-body exposure) for 30 min. This exposure causes 50% mortality (LC₅₀), resulting in 3–4 surviving mice/group (except the control). Male mice were used because previous work by W.K.R. showed that they are more sensitive to acute H₂S exposure than females²⁷. High purity of H₂S gas (>99.9%) or room air (>98%) were supplied from gas cylinders (Airgas, IA). The concentration of H₂S in the exposure chamber was monitored in real-time using a H₂S sensor (RKI Instruments, Union City, CA). Mice were euthanized at 12, 24, 48, and 72 h after the single acute exposure to assess the time course effects of H₂S on mitochondrial morphology. The dose of 1000 ppm was chosen to mimic acute H₂S exposure following industrial accidents or nefarious acts. Only mice surviving acute exposure were used in this study. Mice were euthanized at each time point by decapitation using a guillotine. Mouse brains were immediately removed. The thalamus was micro-dissected on ice, blocked in 1% paraformaldehyde, 3% glutaraldehyde in 0.1 M sodium cacodylate buffer, pH 7.2 at 4 °C, and processed for electron microscopy.

Electron microscopy

Micro-dissected thalamus brain tissues were placed into 1% paraformaldehyde, 3% glutaraldehyde in 0.1 M sodium cacodylate buffer, pH 7.2, and fixed for 48 h at 4 °C. The thalamus tissues were washed in the cacodylate buffer for 10 min three times and post-fixed with 1% osmium tetroxide in 0.1 M sodium cacodylate buffer for one h at 20–22 °C. Subsequently, the thalami were washed thrice with deionized water for 15 min each. The thalamus tissues were washed in distilled water for 10 min and dehydrated through a graded ethanol series (25, 50, 70, 85, 95, 100%) for 1 h each step. This was followed by dehydration, with three changes of pure acetone, 15 min each, and infiltrated with EmBed 812 formula (hard) for EPON epoxy resin (Electron Microscopy Sciences, Hatfield PA) with graded ratios of resin to acetone until thoroughly infiltrated with pure epoxy resin (3:1, 1:1, 1:3, pure) for 6–12 h per step. Thalami were placed into BEEM[®] embedding capsules and polymerized at 70 °C for 48 h. Thick sections (1.5 µm) were made using a Leica UC6 ultramicrotome (Leica Microsystems, Buffalo Grove, IL) and stained with EMS Epoxy stain (a blend of toluidine blue-O and basic fuchsin). Thin sections were made at 50 nm and collected onto single-slot carbon film grids. TEM images were gathered using a 200 kV JEOL JSM 2100 scanning transmission electron microscope (Japan Electron Optics Laboratories, USA, Peabody, MA) with a GATAN One View 4 K camera (Gatan Inc., Pleasanton, CA).

Overall assessment of the brain chondriome and other cellular structures after H₂S exposure

To evaluate the effect of hydrogen sulfide on brain mitochondrial morphology, we assessed 123 images from C57BL/6J male mice, of which 94 were from those mice exposed to H₂S. The observations reported in this study represent approximately 30 min/image for 3900 h performed blindly by three independent reviews and over 400 h of subsequent data analyses.

Morphometry and statistical analyses

Quantitative measurements of a range of common morphometric parameters were performed on individual mitochondria using ImageJ. Object measures, including surface area, were obtained using the methods described before⁷⁶. ANOVA tests followed by Tukey's post-hoc were performed assuming equal or unequal variance based on the F-score, with the level of significance set at 0.05. Statistical analysis was performed using GraphPad Prism (version 7.02).

Effect of NaHS on mitochondrial complex IV activity

Mice in a C57BL/6NJ background were kept in facilities approved by the Association for Assessment and Accreditation of Laboratory Animal Care International (AALAC). The animals were housed in Plexiglas cages (2–4 animals per cage; 55 × 33 × 19) and maintained under standard laboratory conditions (21 ± 2 °C; 55 ± 5% humidity) on a 12 h light/dark cycle, with ad libitum access to both water and food. The mice were fed with a standard rodent chow. All animals were handled by protocols approved by the University of California at Davis Institutional Animal Care and Use Committee. All protocols using animals followed the "Principles of laboratory animal care" (NIH publication No. 86-23, revised 1985). To isolate mitochondria from brains, mice were humanely euthanized by CO₂ inhalation.

All reagents used for this study were of analytical grade or higher. Brain mitochondria from mice (2–3 months old) were utilized for testing the effect of hydrogen sulfide on Complex IV. After euthanasia, whole brains were dissected from the skull and placed in ice-cold PBS buffer to remove excess of blood. Subsequently, mitochondria were isolated by differential centrifugation as described before⁷⁷. Protein was determined by using the BCA method from Pierce.

Mitochondria were evaluated by polarography under phosphorylating and non-phosphorylating conditions with NADH- and FADH₂-linked substrates. Briefly, oxygen consumption was evaluated using a Clark-type oxygen electrode (Hansatech, King's Lynn, UK) as described³¹. Mitochondria (10–20 µg protein) were added to the oxygen chamber in a buffer containing 0.22 M sucrose, 50 mM KCl, 1 mM EDTA, 10 mM KH₂PO₄, and 10 mM

HEPES, pH 7.4. To ensure the quality of these preparations, the oxygen consumption rates were evaluated in the presence of (i) 1 mM malate-10 mM glutamate (State 4) followed by the addition of 1 mM ADP (State 3) or with (ii) 10 mM succinate (State 4) followed by the addition of 1 mM ADP (State 3). This biological preparation's respiratory control ratios (RCR = State 3/State 4) were 5 or above regardless of the substrate, indicating a high coupling between electron transport and ATP production. In situ, specific activity of Complex IV was followed by polarography as described before^{77,78} by assessing the KCN-sensitive oxygen uptake rate by using the artificial substrates ascorbate/TMPD (10 mM/100 μ M, respectively) in the presence of the Complex III inhibitor antimycin at 4 μ M, to evaluate Complex IV only. In separate experiments, various concentrations of NaHS (as a hydrogen sulfide donor) were used to evaluate its effect on Complex IV activity (expressed as nmol oxygen consumed \times (min \times mg mitochondrial protein)⁻¹).

Data availability

The images analyzed during the current study are available in the Dryad repository under the title "Electron microscopy images of the thalamus from acutely hydrogen sulfide poisoned mice" and accessible via the following link: <https://doi.org/10.5061/dryad.k3j9kd5ds>. All data generated and analyzed during this study are included in this published article.

Received: 15 August 2023; Accepted: 12 October 2023

Published online: 24 October 2023

References

- Kimura, H. Hydrogen sulfide (H₂S) and polysulfide (H₂S(n)) signaling: The first 25 years. *Biomolecules*. <https://doi.org/10.3390/biom11060896> (2021).
- Shibuya, N. et al. 3-Mercaptopyruvate sulfurtransferase produces hydrogen sulfide and bound sulfane sulfur in the brain. *Antioxid. Redox Signal* **11**, 703–714. <https://doi.org/10.1089/ars.2008.2253> (2009).
- Kim, J. E. & Kang, T. C. p47Phox/CDK5/DRP1-mediated mitochondrial fission evokes PV cell degeneration in the rat dentate gyrus following status epilepticus. *Front. Cell Neurosci.* **11**, 267. <https://doi.org/10.3389/fncel.2017.00267> (2017).
- DuBoff, B., Gotz, J. & Feany, M. B. Tau promotes neurodegeneration via DRP1 mislocalization in vivo. *Neuron* **75**, 618–632. <https://doi.org/10.1016/j.neuron.2012.06.026> (2012).
- Reddy, P. H. et al. Dynamin-related protein 1 and mitochondrial fragmentation in neurodegenerative diseases. *Brain Res. Rev.* **67**, 103–118. <https://doi.org/10.1016/j.brainresrev.2010.11.004> (2011).
- Zhang, Y., Rui, T., Luo, C. & Li, Q. Mdivi-1 alleviates brain damage and synaptic dysfunction after intracerebral hemorrhage in mice. *Exp. Brain Res.* **239**, 1581–1593. <https://doi.org/10.1007/s00221-021-06089-6> (2021).
- Yang, S., Park, J. H. & Lu, H. C. Axonal energy metabolism, and the effects in aging and neurodegenerative diseases. *Mol. Neurodegener.* **18**, 49. <https://doi.org/10.1186/s13024-023-00634-3> (2023).
- Le Duc, D. et al. Pathogenic WDFY3 variants cause neurodevelopmental disorders and opposing effects on brain size. *Brain* **142**, 2617–2630. <https://doi.org/10.1093/brain/awz198> (2019).
- Giulivi, C., Napoli, E., Tassone, F., Halmaj, J. & Hagerman, R. Plasma biomarkers for monitoring brain pathophysiology in FMR1 premutation carriers. *Front. Mol. Neurosci.* **9**, 71. <https://doi.org/10.3389/fnmol.2016.00071> (2016).
- Daems, W. T. & Wisse, E. Shape and attachment of the cristae mitochondriales in mouse hepatic cell mitochondria. *J. Ultrastruct. Res.* **16**, 123–140. [https://doi.org/10.1016/s0022-5320\(66\)80027-8](https://doi.org/10.1016/s0022-5320(66)80027-8) (1966).
- Frey, T. G. & Mannella, C. A. The internal structure of mitochondria. *Trends Biochem. Sci.* **25**, 319–324. [https://doi.org/10.1016/s0968-0004\(00\)01609-1](https://doi.org/10.1016/s0968-0004(00)01609-1) (2000).
- Perkins, G. et al. Electron tomography of neuronal mitochondria: Three-dimensional structure and organization of cristae and membrane contacts. *J. Struct. Biol.* **119**, 260–272. <https://doi.org/10.1006/jsbi.1997.3885> (1997).
- Cogliati, S. et al. Mitochondrial cristae shape determines respiratory chain supercomplexes assembly and respiratory efficiency. *Cell* **155**, 160–171. <https://doi.org/10.1016/j.cell.2013.08.032> (2013).
- Ernster, L. & Kuylenskierna, B. In *Membranes of Mitochondria and Chloroplasts* (Racker, E. ed.). Vol. 1972 (Van Norstrand Reinhold, 1970).
- Wiemerslage, L. & Lee, D. Quantification of mitochondrial morphology in neurites of dopaminergic neurons using multiple parameters. *J. Neurosci. Methods* **262**, 56–65. <https://doi.org/10.1016/j.jneumeth.2016.01.008> (2016).
- Westrate, L. M., Drocco, J. A., Martin, K. R., Hlavacek, W. S. & MacKeigan, J. P. Mitochondrial morphological features are associated with fission and fusion events. *PLoS One* **9**, e95265. <https://doi.org/10.1371/journal.pone.0095265> (2014).
- Tilokani, L., Nagashima, S., Paupe, V. & Prudent, J. Mitochondrial dynamics: Overview of molecular mechanisms. *Essays Biochem.* **62**, 341–360. <https://doi.org/10.1042/EBC20170104> (2018).
- Haouzi, P., Sonobe, T. & Judenherc-Haouzi, A. Hydrogen sulfide intoxication induced brain injury and methylene blue. *Neurobiol. Dis.* **133**, 104474. <https://doi.org/10.1016/j.nbd.2019.05.013> (2020).
- Rumbeiha, W., Whitley, E., Anantharam, P., Kim, D. S. & Kanthasamy, A. Acute hydrogen sulfide-induced neuropathology and neurological sequelae: Challenges for translational neuroprotective research. *Ann. N. Y. Acad. Sci.* **1378**, 5–16. <https://doi.org/10.1111/nyas.13148> (2016).
- Paul, B. D. & Snyder, S. H. Modes of physiologic H₂S signaling in the brain and peripheral tissues. *Antioxid. Redox Signal* **22**, 411–423. <https://doi.org/10.1089/ars.2014.5917> (2015).
- Kimura, H. Physiological role of hydrogen sulfide and polysulfide in the central nervous system. *Neurochem. Int.* **63**, 492–497. <https://doi.org/10.1016/j.neuint.2013.09.003> (2013).
- Petrovic, D., Kouroussis, E., Vignane, T. & Filipovic, M. R. The role of protein persulfidation in brain aging and neurodegeneration. *Front. Aging Neurosci.* **13**, 674135. <https://doi.org/10.3389/fnagi.2021.674135> (2021).
- Du, A. L. et al. Aminoxyacetic acid improves learning and memory in a rat model of chronic alcoholism. *Neural Regen. Res.* **13**, 1568–1574. <https://doi.org/10.4103/1673-5374.237120> (2018).
- Gabbay, D. S., De Roos, F. & Perrone, J. Twenty-foot fall averts fatality from massive hydrogen sulfide exposure. *J. Emerg. Med.* **20**, 141–144. [https://doi.org/10.1016/s0736-4679\(00\)00301-2](https://doi.org/10.1016/s0736-4679(00)00301-2) (2001).
- Haouzi, P. Ventilatory and metabolic effects of exogenous hydrogen sulfide. *Respir. Physiol. Neurobiol.* **184**, 170–177. <https://doi.org/10.1016/j.resp.2012.05.002> (2012).
- Santana Maldonado, C. M. et al. Acute hydrogen sulfide-induced neurochemical and morphological changes in the brainstem. *Toxicology* **485**, 153424. <https://doi.org/10.1016/j.tox.2023.153424> (2023).
- Anantharam, P. et al. Characterizing a mouse model for evaluation of countermeasures against hydrogen sulfide-induced neurotoxicity and neurological sequelae. *Ann. N. Y. Acad. Sci.* **1400**, 46–64. <https://doi.org/10.1111/nyas.13419> (2017).

28. Doujaiji, B. & Al-Tawfiq, J. A. Hydrogen sulfide exposure in an adult male. *Ann. Saudi Med.* **30**, 76–80. <https://doi.org/10.4103/0256-4947.59379> (2010).
29. Morii, D., Miyagatani, Y., Nakamae, N., Murao, M. & Taniyama, K. Japanese experience of hydrogen sulfide: The suicide craze in 2008. *J. Occup. Med. Toxicol.* **5**, 28. <https://doi.org/10.1186/1745-6673-5-28> (2010).
30. Malone Rubright, S. L., Pearce, L. L. & Peterson, J. Environmental toxicology of hydrogen sulfide. *Nitric Oxide* **71**, 1–13. <https://doi.org/10.1016/j.niox.2017.09.011> (2017).
31. Giulivi, C. *et al.* Mitochondrial dysfunction in autism. *JAMA* **304**, 2389–2396. <https://doi.org/10.1001/jama.2010.1706> (2010).
32. Nicholls, P. The effect of sulphide on cytochrome aa3. Isosteric and allosteric shifts of the reduced alpha-peak. *Biochim. Biophys. Acta* **396**, 24–35. [https://doi.org/10.1016/0005-2728\(75\)90186-3](https://doi.org/10.1016/0005-2728(75)90186-3) (1975).
33. Warena, M. W. *et al.* Acute hydrogen sulfide poisoning. Demonstration of selective uptake of sulfide by the brainstem by measurement of brain sulfide levels. *Biochem. Pharmacol.* **38**, 973–981. [https://doi.org/10.1016/0006-2952\(89\)90288-8](https://doi.org/10.1016/0006-2952(89)90288-8) (1989).
34. Klecker, T., Braun, R. J. & Westermann, B. Lipid droplets guard mitochondria during autophagy. *Dev. Cell* **42**, 1–2. <https://doi.org/10.1016/j.devcel.2017.06.018> (2017).
35. Rai, N. K. *et al.* Exposure to As, Cd and Pb-mixture impairs myelin and axon development in rat brain, optic nerve and retina. *Toxicol. Appl. Pharmacol.* **273**, 242–258. <https://doi.org/10.1016/j.taap.2013.05.003> (2013).
36. Dubinsky, J. M. & Levi, Y. Calcium-induced activation of the mitochondrial permeability transition in hippocampal neurons. *J. Neurosci. Res.* **53**, 728–741. [https://doi.org/10.1002/\(SICI\)1097-4547\(19980915\)53:6%3c728::AID-JNR10%3e3.0.CO;2-U](https://doi.org/10.1002/(SICI)1097-4547(19980915)53:6%3c728::AID-JNR10%3e3.0.CO;2-U) (1998).
37. Brustovetsky, T., Li, V. & Brustovetsky, N. Stimulation of glutamate receptors in cultured hippocampal neurons causes Ca²⁺-dependent mitochondrial contraction. *Cell Calcium* **46**, 18–29. <https://doi.org/10.1016/j.ceca.2009.03.017> (2009).
38. Denton, R. M., Rutter, G. A., Midgley, P. J. & McCormack, J. G. Effects of Ca²⁺ on the activities of the calcium-sensitive dehydrogenases within the mitochondria of mammalian tissues. *J. Cardiovasc. Pharmacol.* **12**(Suppl 5), S69–72 (1988).
39. Rossignol, R. *et al.* Energy substrate modulates mitochondrial structure and oxidative capacity in cancer cells. *Cancer Res.* **64**, 985–993. <https://doi.org/10.1158/0008-5472.can-03-1101> (2004).
40. Bach, D. *et al.* Mitofusin-2 determines mitochondrial network architecture and mitochondrial metabolism. A novel regulatory mechanism altered in obesity. *J. Biol. Chem.* **278**, 17190–17197. <https://doi.org/10.1074/jbc.M212754200> (2003).
41. Quintana, D. D. *et al.* Hypoxia-reoxygenation of primary astrocytes results in a redistribution of mitochondrial size and mitophagy. *Mitochondrion* **47**, 244–255. <https://doi.org/10.1016/j.mito.2018.12.004> (2019).
42. Koopman, W. J. *et al.* Mitochondrial network complexity and pathological decrease in complex I activity are tightly correlated in isolated human complex I deficiency. *Am. J. Physiol. Cell Physiol.* **289**, C881–890. <https://doi.org/10.1152/ajpcell.00104.2005> (2005).
43. Almeida, A. F. & Guidotti, T. L. Differential sensitivity of lung and brain to sulfide exposure: A peripheral mechanism for apnea. *Toxicol. Sci.* **50**, 287–293. <https://doi.org/10.1093/toxsci/50.2.287> (1999).
44. Anantharam, P. *et al.* Cobinamide is effective for treatment of hydrogen sulfide-induced neurological sequelae in a mouse model. *Ann. N. Y. Acad. Sci.* **1408**, 61–78. <https://doi.org/10.1111/nyas.13559> (2017).
45. Bhambhani, Y., Burnham, R., Snyder, G. & MacLean, I. Effects of 10-ppm hydrogen sulfide inhalation in exercising men and women. Cardiovascular, metabolic, and biochemical responses. *J. Occup. Environ. Med.* **39**, 122–129. <https://doi.org/10.1097/00043764-199702000-00009> (1997).
46. Bhambhani, Y., Burnham, R., Snyder, G., MacLean, I. & Martin, T. Effects of 5 ppm hydrogen sulfide inhalation on biochemical properties of skeletal muscle in exercising men and women. *Am. Ind. Hyg. Assoc. J.* **57**, 464–468. <https://doi.org/10.1080/15428119691014819> (1996).
47. Bhambhani, Y. & Singh, M. Physiological effects of hydrogen sulfide inhalation during exercise in healthy men. *J. Appl. Physiol.* **1985**(71), 1872–1877. <https://doi.org/10.1152/jap.1991.71.5.1872> (1991).
48. Brennehan, K. A. *et al.* Olfactory mucosal necrosis in male CD rats following acute inhalation exposure to hydrogen sulfide: Reversibility and the possible role of regional metabolism. *Toxicol. Pathol.* **30**, 200–208. <https://doi.org/10.1080/019262302753559533> (2002).
49. Cochrane, P. V., Rossi, G. S., Tunnah, L., Jonz, M. G. & Wright, P. A. Hydrogen sulphide toxicity and the importance of amphibious behaviour in a mangrove fish inhabiting sulphide-rich habitats. *J. Comp. Physiol. B* **189**, 223–235. <https://doi.org/10.1007/s00360-019-01204-0> (2019).
50. Dorman, D. C. *et al.* Cytochrome oxidase inhibition induced by acute hydrogen sulfide inhalation: Correlation with tissue sulfide concentrations in the rat brain, liver, lung, and nasal epithelium. *Toxicol. Sci.* **65**, 18–25. <https://doi.org/10.1093/toxsci/65.1.18> (2002).
51. Freundt, K. J., Schauenburg, K. J. & Eichhorn, P. Effect of acute exposure to carbon disulfide vapour upon some components of the hepatic-microsomal enzyme system in rats. *Arch. Toxicol.* **32**, 233–240. <https://doi.org/10.1007/BF00318438> (1974).
52. Goyak, K. O. & Lewis, R. J. Application of adverse outcome pathway networks to integrate mechanistic data informing the choice of a point of departure for hydrogen sulfide exposure limits. *Crit. Rev. Toxicol.* **51**, 193–208. <https://doi.org/10.1080/10408444.2021.1897085> (2021).
53. Khan, A. A. *et al.* Effects of hydrogen sulfide exposure on lung mitochondrial respiratory chain enzymes in rats. *Toxicol. Appl. Pharmacol.* **103**, 482–490. [https://doi.org/10.1016/0041-008x\(90\)90321-k](https://doi.org/10.1016/0041-008x(90)90321-k) (1990).
54. Liu, Y. *et al.* Hydrogen sulfide-induced oxidative stress mediated apoptosis via mitochondria pathway in embryo-larval stages of zebrafish. *Ecotoxicol. Environ. Saf.* **239**, 113666. <https://doi.org/10.1016/j.ecoenv.2022.113666> (2022).
55. Roberts, E. S., Thomas, R. S. & Dorman, D. C. Gene expression changes following acute hydrogen sulfide (H₂S)-induced nasal respiratory epithelial injury. *Toxicol. Pathol.* **36**, 560–567. <https://doi.org/10.1177/019262308317422> (2008).
56. Shan, H. *et al.* Neuroprotective effects of hydrogen sulfide on sodium azide-induced autophagic cell death in PC12 cells. *Mol. Med. Rep.* **16**, 5938–5946. <https://doi.org/10.3892/mmr.2017.7363> (2017).
57. Torrans, E. L. & Clemens, H. P. Physiological and biochemical effects of acute exposure of fish to hydrogen sulfide. *Comp. Biochem. Physiol. C Comp. Pharmacol.* **71**, 183–190. [https://doi.org/10.1016/0306-4492\(82\)90034-x](https://doi.org/10.1016/0306-4492(82)90034-x) (1982).
58. Wu, N., Du, X., Wang, D. & Hao, F. Myocardial and lung injuries induced by hydrogen sulfide and the effectiveness of oxygen therapy in rats. *Clin. Toxicol. (Phila)* **49**, 161–166. <https://doi.org/10.3109/15563650.2011.565419> (2011).
59. Nicholls, P. & Kim, J. K. Sulphide as an inhibitor and electron donor for the cytochrome c oxidase system. *Can. J. Biochem.* **60**, 613–623. <https://doi.org/10.1139/o82-076> (1982).
60. Llopis, J., McCaffery, J. M., Miyawaki, A., Farquhar, M. G. & Tsien, R. Y. Measurement of cytosolic, mitochondrial, and Golgi pH in single living cells with green fluorescent proteins. *Proc. Natl. Acad. Sci. USA* **95**, 6803–6808. <https://doi.org/10.1073/pnas.95.12.6803> (1998).
61. Abad, M. F., Di Benedetto, G., Magalhaes, P. J., Filippin, L. & Pozzan, T. Mitochondrial pH monitored by a new engineered green fluorescent protein mutant. *J. Biol. Chem.* **279**, 11521–11529. <https://doi.org/10.1074/jbc.M306766200> (2004).
62. Kalimo, H., Paljarvi, L. & Vapalahti, M. The early ultrastructural alterations in the rabbit cerebral and cerebellar cortex after compression ischaemia. *Neuropathol. Appl. Neurobiol.* **5**, 211–223. <https://doi.org/10.1111/j.1365-2990.1979.tb00620.x> (1979).
63. Pluta, R. Early ultrastructural changes in the basal ganglia, cerebellum and medulla oblongata after complete cerebral ischemia lasting 30 minutes. *Neuropatol. Pol.* **24**, 243–260 (1986).
64. Rambold, A. S., Kostecky, B., Elia, N. & Lippincott-Schwartz, J. Tubular network formation protects mitochondria from autophagosomal degradation during nutrient starvation. *Proc. Natl. Acad. Sci. USA* **108**, 10190–10195. <https://doi.org/10.1073/pnas.1107402108> (2011).

65. Gomes, L. C., Di Benedetto, G. & Scorrano, L. During autophagy mitochondria elongate, are spared from degradation and sustain cell viability. *Nat. Cell Biol.* **13**, 589–598. <https://doi.org/10.1038/ncb2220> (2011).
66. Sun, M. G. *et al.* Correlated three-dimensional light and electron microscopy reveals transformation of mitochondria during apoptosis. *Nat. Cell Biol.* **9**, 1057–1065. <https://doi.org/10.1038/ncb1630> (2007).
67. Caro, A. A., Thompson, S. & Tackett, J. Increased oxidative stress and cytotoxicity by hydrogen sulfide in HepG2 cells overexpressing cytochrome P450 2E1. *Cell Biol. Toxicol.* **27**, 439–453. <https://doi.org/10.1007/s10565-011-9198-2> (2011).
68. Kim, D. S. *et al.* Broad spectrum proteomics analysis of the inferior colliculus following acute hydrogen sulfide exposure. *Toxicol. Appl. Pharmacol.* **355**, 28–42. <https://doi.org/10.1016/j.taap.2018.06.001> (2018).
69. Kilburn, K. H. Exposure to reduced sulfur gases impairs neurobehavioral function. *South Med. J.* **90**, 997–1006. <https://doi.org/10.1097/00007611-199710000-00006> (1997).
70. Mansvelder, H. D., Verhoog, M. B. & Goriounova, N. A. Synaptic plasticity in human cortical circuits: Cellular mechanisms of learning and memory in the human brain?. *Curr. Opin. Neurobiol.* **54**, 186–193. <https://doi.org/10.1016/j.conb.2018.06.013> (2019).
71. Szegei, V. *et al.* Robust perisomatic GABAergic self-innervation inhibits basket cells in the human and mouse supragranular neocortex. *Elife*. <https://doi.org/10.7554/eLife.51691> (2020).
72. Kim, M. H. *et al.* Target cell-specific synaptic dynamics of excitatory to inhibitory neuron connections in supragranular layers of human neocortex. *Elife*. <https://doi.org/10.7554/eLife.81863> (2023).
73. Fujisawa, Y. *et al.* Impact of a novel homozygous mutation in nicotinamide nucleotide transhydrogenase on mitochondrial DNA integrity in a case of familial glucocorticoid deficiency. *BBA Clin.* **3**, 70–78. <https://doi.org/10.1016/j.bbacli.2014.12.003> (2015).
74. Nicholson, A. *et al.* Diet-induced obesity in two C57BL/6 substrains with intact or mutant nicotinamide nucleotide transhydrogenase (Nnt) gene. *Obesity (Silver Spring)* **18**, 1902–1905. <https://doi.org/10.1038/oby.2009.477> (2010).
75. Percie du Sert, N. *et al.* The ARRIVE guidelines 2.0: Updated guidelines for reporting animal research. *PLoS Biol.* **18**, e3000410. <https://doi.org/10.1371/journal.pbio.3000410> (2020).
76. Napoli, E. *et al.* Wdly3 regulates glycolysis, mitophagy, and synaptic plasticity. *J. Cereb. Blood Flow Metab.* **41**, 3213–3231. <https://doi.org/10.1177/0271678X211027384> (2021).
77. Napoli, E. *et al.* Mitochondrial dysfunction in Pten haplo-insufficient mice with social deficits and repetitive behavior: Interplay between Pten and p53. *PLoS One* **7**, e42504. <https://doi.org/10.1371/journal.pone.0042504> (2012).
78. Napoli, E., Hung, C., Wong, S. & Giulivi, C. Toxicity of the flame-retardant BDE-49 on brain mitochondria and neuronal progenitor striatal cells enhanced by a PTEN-deficient background. *Toxicol. Sci.* **132**, 196–210. <https://doi.org/10.1093/toxsci/kfs339> (2013).

Acknowledgements

This study was supported by UC Davis and Iowa State University internal funds to W.K.R. The mitochondrial morphology assessment was funded by discretionary funds (C.G.). We are grateful for the technical assistance of Dr. E. Napoli at the early stages of this project.

Author contributions

Conceptualization, W.K.R.; Methodology, D.K., A.M., M.N., C.G.; Validation, C.G.; Formal Analysis, A.M., M.N., C.G.; Resources, W.K.R. and C.G.; Data Curation, A.M., M.N., C.G.; Writing—Original Draft Preparation, C.G.; Writing—Review & Editing, C.G., W.K.R., D.K.; Supervision, W.K.R. and C.G. All authors have reviewed the manuscript.

Competing interests

No potential financial and non-financial competing interests that could directly or indirectly undermine the objectivity, integrity, and value of this publication through a possible influence on the judgments and actions of authors regarding objective data presentation, analysis, and interpretation were found. C.G. is an Editorial Board Member of *Scientific Reports (Nature Publishing Company)*. She received compensation as Field Chief Editor for *Frontiers in Molecular Biosciences* and honoraria from participating in NIH peer review meetings. W.K.R., D.S.K., A.M., and M.N. have no conflict of interest to report.

Additional information

Supplementary Information The online version contains supplementary material available at <https://doi.org/10.1038/s41598-023-44807-y>.

Correspondence and requests for materials should be addressed to W.K.R. or C.G.

Reprints and permissions information is available at www.nature.com/reprints.

Publisher's note Springer Nature remains neutral with regard to jurisdictional claims in published maps and institutional affiliations.



Open Access This article is licensed under a Creative Commons Attribution 4.0 International License, which permits use, sharing, adaptation, distribution and reproduction in any medium or format, as long as you give appropriate credit to the original author(s) and the source, provide a link to the Creative Commons licence, and indicate if changes were made. The images or other third party material in this article are included in the article's Creative Commons licence, unless indicated otherwise in a credit line to the material. If material is not included in the article's Creative Commons licence and your intended use is not permitted by statutory regulation or exceeds the permitted use, you will need to obtain permission directly from the copyright holder. To view a copy of this licence, visit <http://creativecommons.org/licenses/by/4.0/>.

© The Author(s) 2023